Inorg. Chem. **2007**, *46*, 5076–5083

Triplet State Properties of the OLED Emitter $Ir(btp)_2(acac)$: Characterization by Site-Selective Spectroscopy and Application of High Magnetic Fields

Walter J. Finkenzeller,[†] Thomas Hofbeck,[†] Mark E. Thompson,[‡] and Hartmut Yersin*,[†]

Institut für Physikalische u. Theoretische Chemie, Universität Regensburg, 93053 Regensburg, Germany, and Department of Chemistry, University of Southern California, Los Angeles, California 90089

Received December 1, 2006

The well-known red emitting complex $Ir(btp)_2(acac)$ (bis(2-(2′-benzothienyl)-pyridinato-$N,C^{3'}$)iridium(acetylacetonate)), frequently used as emitter material in OLEDs, has been investigated in a polycrystalline CH_2Cl_2 matrix. The studies were carried out under variation of temperature down to 1.2 K and at magnetic fields up to $B = 10$ T. Highly resolved emission and excitation spectra of several specific sites are obtained by site-selective spectroscopy. For the preferentially investigated site (I → 0 at 16268 cm^{-1}), the three substates I, II, and III of the T_1 triplet state are separated by $\Delta E_{II-I} = 2.9$ cm^{-1} and $\Delta E_{III-I} = 25.0$ cm^{-1}, respectively. ΔE_{III-I} represents the total zero-field splitting (ZFS). The individual decay times of these substates are $\tau_I = 150$ μs, $\tau_{II} = 58$ μs, and $\tau_{III} = 2$ μs, respectively. The long decay time of the lowest substate I indicates its almost pure triplet character. The time for relaxation from state II to state I (spin–lattice relaxation, SLR) is as long as 22 μs at $T = 1.5$ K, while the thermalization between the two lower lying substates and substate III is fast. Application of a magnetic field induces Zeeman mixing of the substates of T_1, resulting in an increased splitting between the two lower lying substates from 2.9 cm^{-1} at zero field to, for example, 6.8 cm^{-1} at $B = 10$ T. Further, the decay time of the *B*-field perturbed lowest substate I_B decreases by a factor of about 7 up to 10 T. The magnetic field properties clearly show that the three investigated states belong to the same triplet parent term of one single site. Other sites show a similar behavior, though the values of ZFS vary between 15 and 27 cm^{-1}. Since the amount of ZFS reflects the extent of MLCT (metal-to-ligand charge transfer) parentage, it can be concluded that the emitting state T_1 is a ^{3}LC (ligand centered) state with significant admixtures of ^{1,3}MLCT (metal-to-ligand charge transfer) character. Interestingly, the results show that the MLCT perturbation is different for the various sites. An empirical correlation between the amount of ZFS and the compound's potential for its use as emitter material in an OLED is presented. As a rule of thumb, a triplet emitter is considered promising for application in OLEDs, if it has a ZFS larger than about 10 cm^{-1}.

1. Introduction

For several years, organometallic phosphorescent compounds have been used as emitters in highly efficient organic light emitting diodes (OLEDs). Application of these materials allows the utilization of both singlet and triplet excitons, which are created by recombination of electrons and holes in the emission layer of an OLED (triplet harvesting).[1−3] One highly attractive triplet emitter complex is $Ir(btp)_2(acac)$,[4−14] first synthesized by Thompson et al.[15] It shows a saturated red emission peaked at about 612 nm,[15−17] close to the

* To whom correspondence should be addressed. E-mail: hartmut.yersin@chemie.uni-regensburg.de.
[†] Universität Regensburg.
[‡] University of Southern California.

(1) Adachi, C.; Baldo, M. A.; Thompson, M. E.; Forrest, S. R. *J. Appl. Phys.* **2001**, *90*, 5048.
(2) Ikai, M.; Tokito, S.; Sakamoto, Y.; Suzuki, T.; Taga, Y. *Appl. Phys. Lett.* **2001**, *79*, 156.
(3) Yersin, H. *Top. Curr. Chem.* **2004**, *241*, 1.
(4) Kawamura, Y.; Goushi, K.; Brooks, J.; Brown, J. J.; Sasabe, H.; Adachi, C. *Appl. Phys. Lett.* **2005**, *86*, 071104.
(5) Tsuboyama, A; IIwawaki, H.; Furugori, M.; Mukaide, T.; Kamatani, J.; IIgawa, S.; Moriyama, T.; Miura, S.; Takiguchi, T.; Okasa, S.; Hoshino, M.; Ueno, K.; *J. Am. Chem. Soc.* **2003**, *125*, 12971.

10.1021/ic0622860 CCC: $37.00
Published on Web 05/09/2007

NTSC[18] standard recommended for video display. Moreover, the emitter material exhibits a high photoluminescence quantum yield of $\Phi_{PL} = 21\%$ in solution with a decay time of 5.8 μs.[15] In a CBP (4,4′-bis(carbazol-9-yl)biphenyl) film, a Φ_{PL} value of even 50% has been reported.[4] Further, the good solubility compared to that of the related tris-cyclometalated compound[19] renders Ir(btp)$_2$(acac) also suitable for solution processing.

Ir(btp)$_2$(acac) has already been investigated as an emitter in different types of devices. For example, efficient red emitting OLEDs have been built with this molecule both by vacuum deposition[15,17,20] and by solution processing.[16,19,21,22] Polymeric devices with linkage of the emitter to a polymer host have been under study.[23−25] In addition to OLEDs incorporating Ir(btp)$_2$(acac), electrogenerated chemiluminescence (ECL) has been demonstrated with the complex.[26−29] Moreover, the feasibility of producing OLEDs on float glass[13] as well as by deposition of the emission layer by spray coating[30] has been studied using Ir(btp)$_2$(acac). Further, several physical investigations have also been carried out, such as UPS and X-ray absorption spectroscopy,[7] and studies of charge transport properties of Ir(btp)$_2$(acac) neat films and Ir(btp)$_2$(acac) doped into a CBP matrix.[31]

These extensive investigations demonstrate the importance of Ir(btp)$_2$(acac). Therefore, it is highly attractive to study the emission properties of this compound. First assignments were presented in ref 15. These were mainly based on ambient temperature broad band emission and absorption spectra of Ir(btp)$_2$(acac) dissolved in Me-THF (2-methyltetrahydrofuran). Although the emitting triplet has already been assigned to be of ligand centered $\pi\pi^*$ character with MLCT admixtures, more detailed information is desirable. Indeed, in recent studies, it could be demonstrated that highly resolved emission and excitation spectra are attainable.[32,33] Thus, a deep insight into the compound's electronic properties can be gained. In this publication, we study the electronic structure of the emitting triplet of Ir(btp)$_2$(acac) by high-resolution site-selective spectroscopy at low temperatures and under application of magnetic fields. We investigate the emission behavior, in particular with respect to the transitions between the three triplet substates and the electronic ground state S_0, the zero-field splitting (ZFS), and the tunability of properties by application of high magnetic fields. Especially, the value of ZFS allows us to make an assessment of the MLCT character in the emitting triplet state with respect to an application of Ir(btp)$_2$(acac) as an emitter material in OLEDs.

2. Experimental Section

Synthesis. Ir(btp)$_2$(acac) was synthesized according to the procedure described in ref 15.

Spectroscopy. Spectroscopic measurements were carried out with Ir(btp)$_2$(acac) in CH_2Cl_2 and in n-octane, respectively, at concentrations of 10^{-5} mol/L. For comparison, also Ir(btp)$_2$(acac) single crystals were studied. Absorption spectra were recorded with a Varian Cary 300 double beam spectrometer. Emission and excitation spectra at 300 and 77 K were measured with a steady-state fluorescence spectrometer (Jobin Yvon Fluorolog 2). Experiments at lower temperatures were carried out in a He cryostat (Cryovac Konti Kryostat IT) in which He gas flow, pressure, and heating were controlled. For magnetic field experiments, a cryostat equipped with a 12/14 T magnet was used. A UV diode laser (Toptica IBeam, 373 nm) or an Ar^+ laser (Coherent Innova 90) was used as source for nonselective excitation. For site-selective excitation, a pulsed dye laser (Lambdaphysik Scanmate 2C) was operated using Rhodamine B and Rhodamine 101, respectively. The spectra were recorded with an intensified CCD camera (Princeton PIMAX) or a cooled photomultiplier (RCA C7164R), both attached to a triple spectrograph (S&I Trivista TR 555). The phosphorescence light was imaged onto the entrance slit of the spectrometer via a two-lens optic and a pinhole. For CCD measurements, the spectrograph was operated with the first two stages in a subtractive mode to optimize stray light rejection. Decay times were measured using a

(6) Tanaka, I.; Tabata, Y.; Tokito, S. *Jpn. J. Appl. Phys.* **2004**, *43*, L1601.
(7) Thompson, J.; Arima, V.; Matino, F.; Berkebile, S.; Koller, G.; Netzer, F. P.; Ramsey, M. G.; Cingolani, R.; Blyth, R. I. R. *Synth. Met.* **2005**, *153*, 233.
(8) Evans, N. R.; Devi, L. S.; Mak, C. S. K.; Watkins, S. E.; Pascu, S. I.; Köhler, A.; Friend, R. H.; Williams, C. K.; Holmes, A. B. *J. Am. Chem. Soc.* **2006**, *128*, 6647.
(9) Kawamura, Y.; Brooks, J.; Brown, J. J.; Sasabe, H.; Adachi, C. *Phys. Rev. Lett.* **2006**, *96*, 17404.
(10) Sudhakar, M.; Djurovich, P. I.; Hogen-Esch, T. E.; Thompson, M. E. *J. Am. Chem. Soc.* **2003**, *125*, 7796.
(11) D'Andrade, B. D.; Thompson, M. E.; Forrest, S. R. *Adv. Mater.* **2002**, *14*, 147.
(12) Tokito, S.; Iijima, T.; Tsuzuki, T.; Sato, F. *Appl. Phys. Lett.* **2003**, *83*, 2459.
(13) Maiorano, V.; Perrone, E.; Carallo, S.; Biasco, A.; Pompa, P. P.; Cingolani, R.; Croce, A.; Blyth, R. I. R.; Thompson, J. *Synth. Met.* **2005**, *151*, 147.
(14) Jou, J. H.; Sun, M. C.; Chou, H. H.; Li, C. H. *Appl. Phys. Lett.* **2005**, *87*, 043508.
(15) Lamansky, S.; Djurovich, P.; Murphy, D.; Abdel-Razzaq, F.; Lee, H.-E.; Adachi, C.; Burrows, P. E.; Forrest, S. R.; Thompson, M. E. *J. Am. Chem. Soc.* **2001**, *123*, 4304.
(16) Chen, F. C.; Yang, Y.; Thompson, M. E.; Kido, J. *Appl. Phys. Lett.* **2003**, *80*, 2308.
(17) Adachi, C.; Baldo, M. A.; Forrest, S. R.; Lamansky, S.; Thompson, M. E.; Kwong, R. C. *Appl. Phys. Lett.* **2001**, *78*, 1622.
(18) NTSC = National Television System Committee.
(19) Lamansky, S.; Djurovich, P. I.; Abdel-Razzaq, F.; Garon, S.; Murphy, D.; Thompson, M. E. *J. Appl. Phys.* **2002**, *92*, 1570.
(20) Moon, D. G.; Pode, R. B.; Lee, C. J.; Han, J. I. *Mater. Sci. Eng., B* **2005**, *121*, 232.
(21) Chen, F. C.; Chang, S. C.; He, G.; Pyo, S.; Yang, Y.; Kurotaki, M.; Kido, J. *J. Polym. Sci., Part B: Polym. Phys.* **2003**, *41*, 2681.
(22) Tokito, S.; Suzuki, M.; Sato, F.; Kamachi, M.; Shirane, S. *Org. Electron.* **2003**, *4*, 105.
(23) Chen, X.; Liao, J.-L.; Liang, Y.; Ahmed, M. O.; Tseng, H.-E.; Chen, S.-A. *J. Am. Chem. Soc.* **2003**, *125*, 636.
(24) Tokito, S.; Suzuki, M.; Sato, F. *Thin Solid Films* **2003**, *445*, 353.
(25) Sandee, A. J.; Williams, C. K.; Evans, N. R.; Davies, J. E.; Boothby, C. E.; Köhler, A.; Friend, R. H.; Holmes, A. B. *J. Am. Chem. Soc.* **2004**, *126*, 7041.
(26) Chen, F.-C.; Yang, Y.; Pei, Q. *Appl. Phys. Lett.* **2002**, *81*, 4278.
(27) Muegge, B. D.; Richter, M. M. *Anal. Chem.* **2004**, *76*, 73.
(28) Kapturkiewicz, A.; Nowacki, J.; Borowicz, P. *Electrochim. Acta* **2005**, *50*, 3395.
(29) Muegge, B. D.; Richter, M. M. *Luminescence* **2005**, *20*, 76.
(30) Echigo, T.; Naka, S.; Okada, H.; Onnagawa, H. *Jpn. J. Appl. Phys.* **2005**, *44*, 626.
(31) Matsusue, N.; Suzuki, Y.; Naito, H. *Jpn. J. Appl. Phys.* **2005**, *44*, 3691.
(32) Yersin, H.; Finkenzeller, W.; Thompson, M. E. *16th ISPPCC Conference*; Asilomar, CA, 2005; Book of Abstracts, O-27, and *SPIE Optics & Photonics*; San Diego, CA, 2005, Book of Abstracts, 5214 (Organic Light-Emitting Materials and Devices VII).
(33) Marchetti, A. P.; Deaton, J. C.; Young, R. H. *J. Phys. Chem. A* **2006**, *110*, 9828.

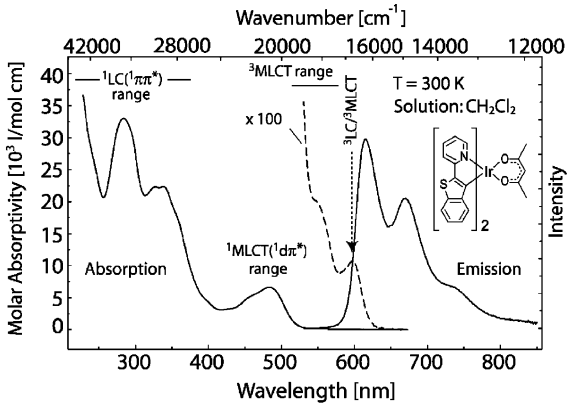

Figure 1. Absorption and emission spectrum of $Ir(btp)_2(acac)$ in CH_2Cl_2 under ambient conditions. The dashed line shows the absorption in the region of the lowest excited states scaled by a factor of 100. The emission spectrum was measured at a concentration of about 10^{-5} mol/L under cw excitation at 480 nm. The assignments given should not be taken too strictly, i.e., states designated as ^{1,3}LC and ^{1,3}MLCT contain also contributions of $d\pi^*$ and $\pi\pi^*$ character, respectively.

FAST Comtec (München) multichannel scaler PCI-card with time resolution of 250 ps.

3. Results and Discussion

3.1. Spectroscopic Introduction. Figure 1 shows the absorption and the emission spectrum of $Ir(btp)_2(acac)$ measured under ambient conditions. The observed transitions are assigned in accordance with the literature[15] and in analogy to the assignments of the recently investigated compounds $Ir(ppy)_3$[34] and $Ir(ppy)_2(CO)(Cl)$.[35]

Strong transitions in the wavelength region below ≈350 nm (28570 cm^{-1}) are assigned to be largely of LC (ligand centered) (btp)$\pi\pi^*$ character. Maxima are observed at 284 nm (35210 cm^{-1}, ϵ_{max} = 33000 L mol^{-1} cm^{-1}), 327 nm (30580 cm, ϵ_{max} = 22250 L mol^{-1} cm^{-1}), and 339 nm (29500 cm^{-1}, ϵ_{max} = 22350 L mol^{-1} cm^{-1}). The absorption between 410 and 535 nm with its maximum at 484 nm (20660 cm^{-1}, ϵ_{max} = 6300 L mol^{-1} cm^{-1}) is assigned to transitions from the singlet ground state to states with strong MLCT (Ir5d−(btp)π^*) contributions. Weak transitions in the long wavelength region of the absorption are scaled by a factor of 100 in Figure 1 (dashed line). Two weak bands at 552 nm (shoulder, 18115 cm^{-1}, ϵ_{max} estimated to 60 L mol^{-1} cm^{-1}) and 598 nm (16720 cm^{-1}, ϵ_{max} ≈ 80 L mol^{-1} cm^{-1}) represent absorptions related to the lowest triplet. Due to the resonance between absorption and emission, the peak at 598 nm corresponds to the electronic origins of the T_1 state (for details, see section 3.3). The shoulder at 552 nm exhibits an energy separation to the peak at 598 nm of ≈1400 cm^{-1}. Therefore, it might correspond to vibrational satellites. Indeed, the structure of the 300 K emission spectrum shows an equivalent peak at 1385 cm^{-1} relative to the electronic origin, which can safely be assigned to (several overlapping) vibrational satellites (see below). The fact that the absorption into the lowest triplet state T_1 is observed is remarkable and is indicative of an MLCT admixture to this state.

An excitation spectrum recorded at 77 K (not depicted) shows a few additional features due to a slightly better resolution. Especially, an additional shoulder is observed at 517 nm (19340 cm^{-1}), with a significant molar extinction of roughly 1200 L mol^{-1} cm^{-1}. This shoulder is tentatively assigned to a higher lying state featuring a larger MLCT contribution than the T_1 state. The assignment is in agreement with the interpretation given for $Ir(ppy)_3$ which shows a similar structure in the region of the ^{1}MLCT/^{3}MLCT ↔ S_0 (state 0) transitions.[35−37] In this context, it is important to note that due to mixing of states by spin−orbit coupling an assignment as either singlet or triplet is only a guideline.

The 300 K emission spectrum of $Ir(btp)_2(acac)$ measured in CH_2Cl_2 shows four bands. The maximum lies at 615 nm (16260 cm^1). This band is related to the electronic origin transitions broadened inhomogeneously and by electron−phonon coupling (see also section 3.2). Further peaks are found at 670 nm (14925 cm^{-1}), at 738 nm (13550 cm^{-1}), and a weak one at 825 nm (12120 cm^{-1}). These are ascribed to overlapping vibrational satellites which form a progression-like structure. Indeed, at low temperature, progressions of 1401 and 1478 cm^{-1} are observed (compare ref 38). The structure of the emission spectrum is again indicative of some MLCT admixture to a ^{3}LC state. On the other hand, a very high degree of metal participation in the lowest triplet would induce intense metal−ligand vibrational satellites in the spectral region below 500 cm^{-1}. This would lead to a more pronounced smearing out or spectral broadening than observed for $Ir(btp)_2(acac)$.(Compare, for example, the spectra of $Ir(ppy)_3$.[34]) On the other hand, the observed widths of the different emission bands are significantly larger than usually found for ^{3}LC emitters.[39]

3.2. Low-Temperature Spectra and Site Distribution. Figure 2 shows the emission spectrum of $Ir(btp)_2(acac)$ in CH_2Cl_2 recorded at 4.2 K in comparison to the spectrum measured at 77 K. Both spectra were recorded using UV excitation (λ_{exc} = 363.8 nm).

While at 77 K the spectrum consists only of broad bands of half-widths of about 500 cm^{-1}, cooling to 4.2 K reveals a manifold of narrow lines of half-widths of only a few cm^{-1} and a broad background. Both the narrow lines as well as the background of the 4.2 K spectrum can be explained taking into account that the $Ir(btp)_2(acac)$ dopant molecules can experience dissimilar interactions with their respective environment in the host matrix. Different orientations of the dopants within the matrix (host) cage and/or a different number of host molecules that are being replaced cause dissimilar shifts and/or splittings of the electronic states. For a large number of molecules, a broad inhomogeneous distribution of transition energies results, and one observes unresolved emission. The broad background of the 4.2 K emission spectrum in Figure 2 is explained in these terms. On the other hand, specific energy minima can exist for

(34) Finkenzeller, W. J.; Yersin, H. *Chem. Phys. Lett.* **2003**, *377*, 299.
(35) Finkenzeller, W. J.; Stössel, P.; Yersin, H. *Chem. Phys. Lett.* **2004**, *397*, 289.
(36) Colombo, M. G.; Güdel, H. U. *Inorg. Chem.* **1993**, *32*, 3081.
(37) King, K. A.; Spellane, P. J.; Watts, R. J. *J. Am. Chem. Soc.* **1985**, *107*, 1431.
(38) Finkenzeller, W. J.; Thompson, M. E.; Yersin, H. Submitted.
(39) Yersin, H.; Donges, D. *Top. Curr. Chem.* **2001**, *214*, 82.

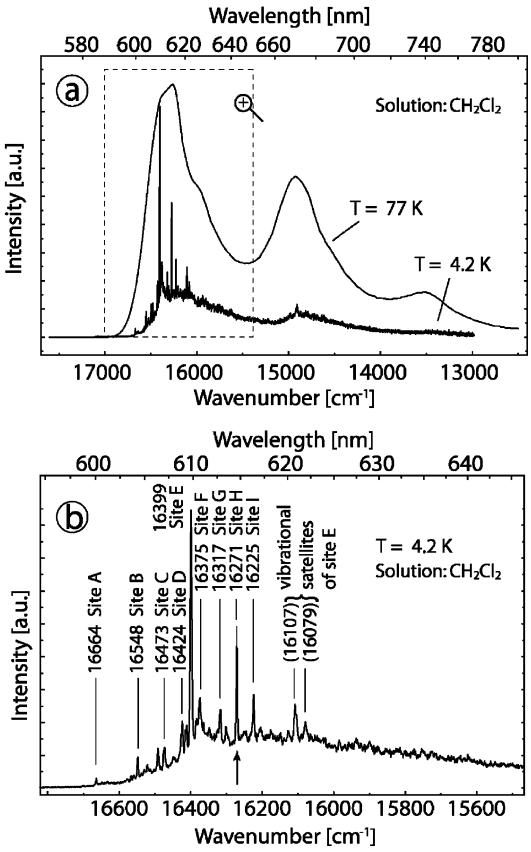

Figure 2. (a) Comparison of the emission spectra of Ir(btp)$_2$(acac) in CH_2Cl_2 (10^{-5} mol/L) recorded at 77 and 4.2 K, respectively, excited at λ_{exc} = 363.8 nm. At 77 K, the spectrum is still unresolved due to inhomogeneous broadening and homogeneous broadening by electron−phonon coupling. The 4.2 K spectrum shows a site structure consisting mainly of highly resolved electronic 0−0 lines and an intense inhomogeneous background. (b) Magnified region of the 4.2 K emission framed in part a. All lines labeled with capital letters represent electronic origins (T_1 substate II → ground state S_0) of different sites. In particular, site H at 16271 cm^{-1} (arrow in part b) will be subject to detailed investigations in the following sections.

molecules doped into the matrix. This leads to the formation of discrete sites, each occupied by a larger number of molecules. Correspondingly, narrow lines can occur. The 4.2 K spectrum depicted in Figure 2a and enlarged in Figure 2b shows a number of such lines. Each is related to one specific and discrete site.

Most of the narrow lines in the 4.2 K emission spectrum represent electronic 0−0 transitions from substate II of the lowest triplet state T_1 to the ground state S_0. This is indicated by the fact that at the corresponding energies the respective molecules can be excited resonantly and selectively (for details, see also below). The distribution of sites found for Ir(btp)$_2$(acac) doped into CH_2Cl_2 spans a width of about 450 cm^{-1}. The different sites are labeled with capitals in Figure 2. The main site is located at 16399 cm^{-1} (site E). Weaker sites are found blue-shifted to the main site at least up to 16664 cm^{-1} and red-shifted at least down to 16225 cm^{-1}. Table 1 summarizes some data on the different sites of Ir(btp)$_2$(acac) in CH_2Cl_2 including the energies of the three triplet substates, zero-field splitting values, and relative intensities. (Compare the explanations given in section 3.3.) The corresponding data are also given for the main site found in n-octane and in single crystals of Ir(btp)$_2$(acac).

For completeness, we address the question of why the resolution is lost as the temperature is increased from 4.2 to 77 K (Figure 2a). This is due to temperature dependent (homogeneous) broadening caused by electron−phonon interaction: Low-energy vibrations of the dopant in its lattice cage (local phonons) couple to the purely electronic and the vibronic transitions. This leads to the appearance of phonon sidebands (satellites), which accompany the zero-phonon lines and are spectrally much broader than these. With increasing temperature, the phonon sidebands gain intensity at the expense of the intensities of the zero-phonon lines.[40] Moreover, the zero-phonon lines themselves (electronic origins or vibrational satellites) are broadened with temperature increase due to thermally activated phonon 1−1 transitions, 2−2 transitions, etc., which have slightly different energies than the 0−0 transitions due to the differences of the force constants in the electronic ground state as compared to the triplet state. At 77 K, for example, the spectral features of the discrete sites have become too broad and overlap, and thus, cannot be distinguished from the inhomogeneous background (compare Figure 2a). Hence, an unresolved spectrum results, which is similar to the shape of the inhomogeneous background of the 4.2 K spectrum.

3.3. Electronic Origins and Energy Level Diagram. Using a tunable laser, a specific site can be studied individually by selective excitation, i.e., by resonantly exciting the corresponding molecules. One specific site exhibiting an electronic origin at 16271 cm^{-1} (site H) is the most suitable one for this investigation. It is located in the longer wavelength region of the distribution. Thus, an excitation at this energy prevents the unintentional excitation of other sites. Furthermore, due to the high relative intensity of site H, its emission is well detectable. Figure 3 shows a selected excitation spectrum and emission spectra in the range of the 0−0 transitions for different temperatures.

Three lines are observed. It will be shown below that they represent purely electronic 0−0 transitions between the T_1 substates I, II, and III, and the ground state 0 (S_0). The purely electronic nature is substantiated by the fact that the transitions exhibit the same energy in excitation and emission. Moreover, the experiments carried out under application of high magnetic fields demonstrate that these three lines belong to the same triplet parent term (see section 3.4). The spectra reveal that the substates I and II are separated by (2.9 ± 0.2) cm^{-1}, whereas the splitting of substates I and III, which represents the total zero-field splitting, amounts to (25.0 ± 0.5) cm^{-1}. According to the extensive investigations by Yersin et al.[3,39] and the ordering scheme which correlates ZFS values and MLCT character, this value of ΔE_{III-I} shows that the T_1 state does not represent a pure ^{3}LC state. It is strongly perturbed by MLCT admixtures.

Figure 3b shows emission spectra of Ir(btp)$_2$(acac) in the region of the electronic origins recorded at temperatures between 1.35 and 20 K. These spectra of site H are selectively excited at 16742 cm^{-1}. This energy corresponds

(40) *Zero-Phonon Lines and Spectral Hole Burning in Spectroscopy and Photochemistry*; Sild, O., Haller, K., Eds.; Springer-Verlag: Berlin, 1988.

Table 1. Transition Energies and Zero-Field Splittings for the Various Sites of $Ir(btp)_2(acac)$ Doped into CH_2Cl_2 and n-Octane and for Single Crystals of $Ir(btp)_2(acac)$[a]

			spectral position [cm^{-1}]			ZFS [cm^{-1}]	
matrix	site	relative intensity	I	II	III	ΔE_{II-I}	ΔE_{III-I}
CH_2CH_2	A	0.03		16664			
	B	0.09		16548	16566		≈21
	C	0.08	16470	16473	16488	3.2 ± 0.5	17.5 ± 1
	D	0.14	16422	16424	16445	2.2 ± 0.5	23.0 ± 0.5
	E	1	16396	16399	16411	2.9 ± 0.2	14.8 ± 0.5
	F	0.12		16375	≈16395		≈23
	G	0.12	16314	16317	16333	3.7 ± 1	19 ± 3
	H	**0.49**	**16268**	**16271**	**16293**	**2.9 ± 0.2**	**25.0 ± 0.5**
	I	0.19	16221	16225	16247	3.6 ± 0.3	26.5 ± 1
n-octane	A	0.89	16198	16201	16224	2.5 ± 0.2	25.3 ± 0.5
single crystal			16293	16296	16312	3.4 ± 0.4	19 ± 1

[a] In part, the ZFS values can be given with higher accuracy, since they are determined as energy differences. In this paper, mainly site H is investigated (see below). The data given for the other sites have been determined in a similar manner.

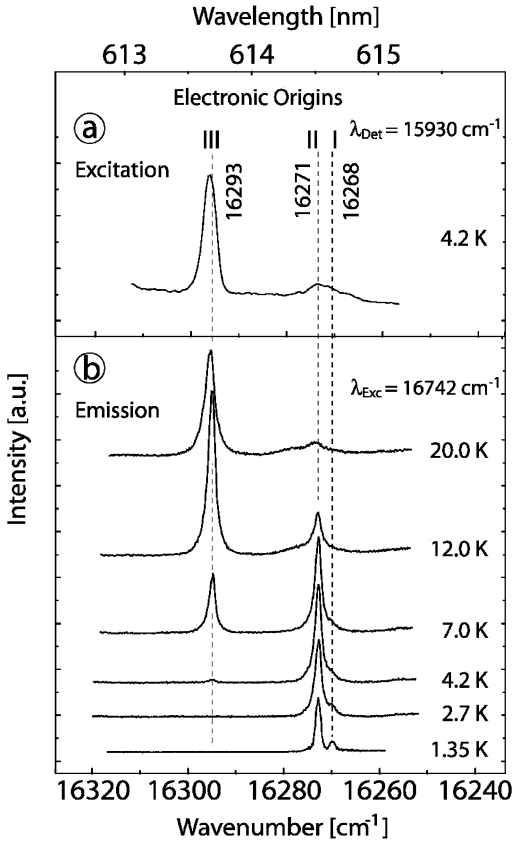

Figure 3. (a) Excitation spectrum in the region of the electronic origins recorded at 4.2 K. The emission is detected on a vibrational satellite of the II → 0 transition at 15930 cm^{-1} (341 cm^{-1} vibration). (b) Emission in the region of the electronic origins recorded at different temperatures under excitation into a vibrational satellite of the 0 → III transition at 16742 cm^{-1} (449 cm^{-1} vibration). The intensities of the different spectra are comparable. The spectrum at $T = 1.35$ K was recorded with higher resolution to obtain the energy difference ΔE_{II-I} between substates I and II. The energy values given in part a are rounded to 1 cm^{-1} corresponding to the accuracy of the absolute wavenumber. The relative accuracy can be as high as ±0.2 cm^{-1}.

to a vibrational satellite of $\bar{\nu} = 449$ cm^{-1} to the 0 → III transition. The spectrum at 1.35 K shows clearly two close-lying lines at 16271 cm^{-1} and at 16268 cm^{-1} corresponding to the transitions II → 0 and I → 0, respectively. With temperature increase, emission I → 0 becomes weaker and is not detectable above 10 K, while the line originating from state II gains intensity up to about 5 K. Near 5 K, a third line appears at 16293 cm^{-1}. It is assigned to the 0−0

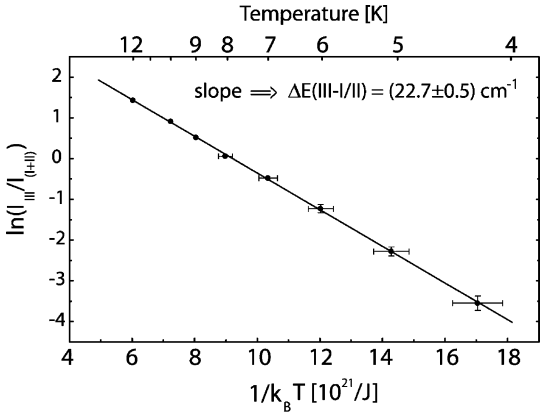

Figure 4. Logarithmic plot of the intensity ratio of the emission from substate III relative to the sum of the intensities of substates I and II versus $1/k_BT$. The slope of the linear fit reveals an energy separation of (22.7 ± 0.5) cm^{-1}.

transition III → 0. With a further temperature increase up to 20 K, the intensity of this line III increases drastically, while the line at 16271 cm^{-1} corresponding to transition II → 0 loses intensity. Heating up to higher temperatures, e.g. to 50 K, does not reveal any higher lying state.

Figure 4 summarizes the intensity ratios of the electronic origin lines in a Boltzmann plot. The experimental data can nicely be fitted by equation

$$\ln\left(\frac{I_{III}}{I_{I+II}}\right) = \text{const} + \frac{-\Delta E_{III-I/II}}{k_B T} \qquad (1)$$

wherein I_{III} and I_{I+II} represent the intensities resulting from substate III and the sum of the intensities from substates I and II, respectively. The sum is used as the resolution of the measured spectra for $T \geq 2$ K does not allow to treat the corresponding lines separately with sufficient accuracy. $\Delta E_{III-I/II}$ is the energy separation between the substates I/II and III and k_B is the Boltzmann constant. The fit gives an energy separation of (22.7 ± 0.5) cm^{-1}. This value reproduces the average of the splittings ΔE_{III-I} and ΔE_{III-II} which we determined independently by high-resolution experiments (see Figure 3). The result obtained is of particular interest. Application of eq 1 is only allowed if the thermal equilibration between state III and the states I/II is fast.[41−43] Obviously, this is fulfilled for processes III ↔ I and III ↔

II. Therefore, we can conclude that the lines observed in Figure 3 result from states which belong to one single site and are intrinsic to the molecules of this ensemble. An alternative interpretation in which the three lines would be assigned to different sites would not hold, since at concentrations of $\approx 10^{-5}$ mol/L fast processes of energy transfer between states of different sites are not expected to occur. The conclusion that the three states belong to the same molecule follows also from the investigations under high magnetic fields (see section 3.4). For completeness, it is remarked that the equilibration between substates I and II is very slow at low temperature. The corresponding spin−lattice relaxation (SLR) time is as long as 22 μs at 1.5 K.[38] Therefore, the Boltzmann distribution is not established for these two substates II and I at low temperature. As a consequence, the emission from substate II cannot be frozen out. (Compare also to the review.[44])

The excitation spectrum presented in Figure 3a demonstrates that transition 0 → III exhibits the highest oscillator strength, while transition 0 → II shows a significantly lower intensity. Transition 0 → I is very weak. Since the excitation intensities reflect the oscillator strengths and since these are proportional to the radiative rates, one expects a similar trend for the individual decay times of the substates I, II, and III. Indeed, they are determined in ref 38 to be $\tau_I = (150 \pm 5)$ μs, $\tau_{II} = (58 \pm 3)$ μs, and $\tau_{III} = (2 \pm 1)$ μs, respectively. The long emission decay time of τ_I is an indication of an almost pure triplet character of substate I, while the short decay time of state III indicates at least a small singlet component mixed in (compare ref 45). This is in agreement to a recent theoretical investigation by Nozaki.[46] In this study, using a strongly simplified model for Ir(ppy)$_3$, it is shown that substate I is largely a pure triplet state, while the substates II and III contain singlet contributions of the order of 1%. Figure 5 summarizes the data obtained for Ir(btp)$_2$(acac) in CH_2Cl_2 (site H) in an energy level diagram.

3.4. Magnetic Field Effects. In order to obtain further evidence that the three states I, II, and III represent substates of one triplet state, Ir(btp)$_2$(acac) is also investigated under high magnetic field. Figure 6 shows the emission lines of Ir(btp)$_2$(acac) in CH_2Cl_2 (site H) in the energy range of the electronic origin transitions I → 0 and II → 0 at different magnetic flux densities between $B = 0$ T and $B = 6$ T. The spectra were recorded at a temperature of $T = 2.8$ K under selective excitation of substate III. The excitation energy was 16293 cm^{-1} at $B = 0$ T, and it was blue-shifted stepwise with field increase by ≈ 0.2 cm^{-1} per Tesla to match the energy of the corresponding transition at the respective field. Figure 7 summarizes the magnetic field induced energy shifts of the three electronic origins.

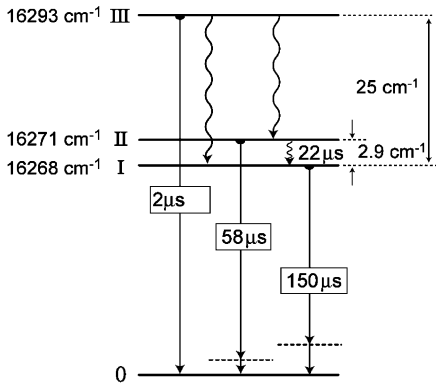

Figure 5. Energy level diagram and photophysical data for the lowest triplet state T_1 of Ir(btp)$_2$(acac). The state is classified as ^{3}LC state which is strongly MLCT perturbed. The values given apply to the specific site under investigation (site H in Figure 2b). Other sites display different values (compare Table 1). After excitation of triplet substate III, the relaxation to the lower lying substates (spin−lattice relaxation, SLR) is fast even at $T = 1.2$ K. However, the relaxation time between the substates II and I is extremely long and amounts to $\tau_{SLR} = 22$ μs at $T = 1.5$ K. This value and the individual decay times are determined in ref 38 and are given here for completeness. The dashed lines represent vibrational levels, which are usually also involved in the emission processes.

With an increase of the magnetic field strength, distinct Zeeman shifts of the transition energies are observed. While the splitting between substates I and II at $B = 0$ T amounts to 2.9 cm^{-1}, it is increased to 4.8 cm^{-1} at $B = 6$ T and to 6.8 cm^{-1} at $B = 10$ T. (The 8 and the 10 T spectrum are not depicted in the series of Figure 6, as they have been recorded at $T = 14$ K to obtain sufficient thermal population of the magnetically perturbed substate II$_B$.) The Zeeman shift is not symmetric. At $B = 8$ T, the energy separation between the substates I and II is increased by 3.1 cm^{-1}, whereas the separation between the states II and III is enhanced only by 1.5 cm^{-1}. These asymmetric Zeeman shifts are qualitatively understood since the *B*-field induced mixings between the corresponding energy states depend on their energy separations at zero field (energy denominators) which are strongly asymmetric for Ir(btp)$_2$(acac). For completeness, it has to be remarked that the Zeeman shifts can be quite different for molecules with different orientations relative to the magnetic field vector. This applies also to polycrystalline samples, as the molecules of one specific site have different orientations for the different microcrystals. Therefore, the observed Zeeman pattern represents an average for distributed orientations. A corresponding quantitative analysis is not presented in this case, but has been carried out, for example, for Pt(thpy)$_2$ (thpy = 2-(2′-thienyl)pyridinato-*N*,*C*$^{5'}$) in ref 47.

An additional effect of application of the magnetic field becomes apparent in the spectra of Figure 6. At $B = 0$ T, the transition from substate I to the ground state 0 is very weak. With increase of the field strength, it gains significant intensity. This effect becomes obvious already for $B < 1$ T (not shown). At 2 T, the intensity stemming from the perturbed state I$_B$ is almost equal to that of transition II$_B$ → 0 which, in return, loses intensity upon increase of the magnetic field strength. At $B = 6$ T, for example, the

(41) Harrigan, R. W.; Crosby, G. A. *J. Chem. Phys.* **1973**, *59*, 3468.
(42) Azumi, T.; O'Donnell, C. M.; McGlynn, S. P. *J. Chem. Phys.* **1966**, *45*, 2735.
(43) Strasser, J.; Homeier, H. H. H.; Yersin, H. *Chem. Phys.* **2000**, *255*, 301.
(44) Yersin, H.; Strasser, J. *Coord. Chem. Rev.* **2000**, *208*, 331.
(45) Yersin, H.; Finkenzeller, W. In *Highly Efficient OLEDs with Phosphorescent Materials*; Yersin, H., Ed.; Wiley-VCH: Weinheim, 2007.
(46) Nozaki, K. *J. Chin. Chem. Soc.* **2006**, *53*, 101.
(47) Strasser, J. Ph.D. Thesis, Universität Regensburg, 1999.

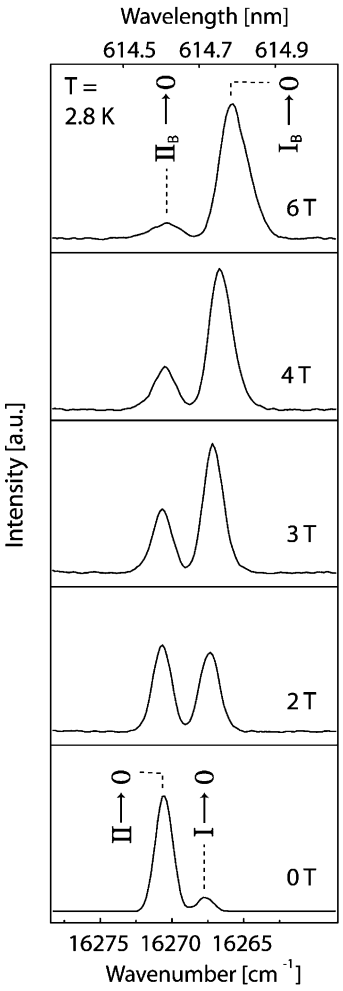

Figure 6. Emission spectra of site H in the region of the electronic origins of I → 0 and II → 0 at different magnetic field strengths. With increasing field strength, the emission from the magnetically perturbed state I_B gains significant intensity. All spectra were recorded at 2.8 K. For selective excitation, transition 0 → III with an energy of 16293 cm^{-1} at $B = 0$ T was used. However, with increasing field strength the excitation was stepwise shifted to higher energy to account for the field-induced blue shift of substate III. At $B = 6$ T, the excitation energy was 16294 cm^{-1}.

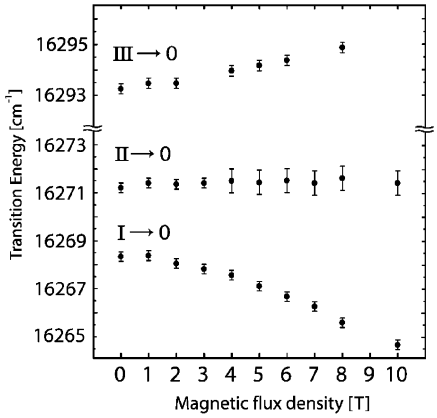

Figure 7. Magnetic field induced shifts of the T_1 substates I, II, and III of $Ir(btp)_2(acac)$ in CH_2Cl_2 (site H). The data are extracted from emission spectra recorded at various temperatures in the range from 2.8 to 14 K. The emission lines corresponding to transition $I_B \rightarrow 0$ were determined at $T = 2.8$ K, while the emission from the substates II_B and III_B was measured at 8 and 14 K, respectively. The higher temperature was chosen to provide sufficient population of these states. For recording emission from substates I and II, substate III was excited, while emission from substate **III** was measured under excitation into a vibrational satellite of substate III ($\bar{\nu}_{exc} =$ 16742 cm^{-1} at $B = 0$ T). Selective excitation was always tuned with increasing magnetic field strength to match the excitation energy of the Zeeman shifted state III.

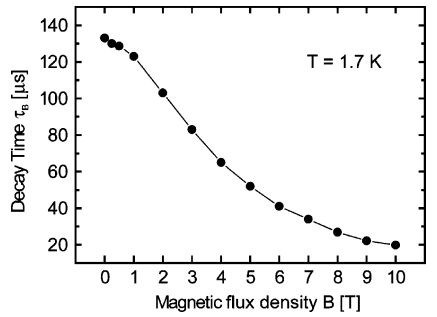

Figure 8. Emission decay time of $Ir(btp)_2(acac)$ in CH_2Cl_2 (site H). The decay time is measured for different magnetic flux densities B at $T = 1.7$ K and under selective excitation of T_1 substate III. The decay behavior is monoexponential in the whole range $0 \leq B \leq 10$ T.

intensity of transition $I_B \rightarrow 0$ dominates clearly. For an explanation of this effect, three factors are of importance. First, the magnetic field-induced mixing of the wavefunction of substate I with the wavefunctions of the two higher states renders transition $I_B \rightarrow 0$ more allowed. Second, due to the increased splitting between substates I and II under magnetic field, the Boltzmann factor for population of state II **(**relative to state I**)** is significantly smaller. Third, spin−lattice relaxation between the triplet substates becomes considerably faster with increasing field-induced energy separation between the corresponding states (compare refs 39 and 44). Accordingly, the Boltzmann distribution is established faster, and thus, the nonequilibrated fraction of the emission resulting from the higher lying substate II_B is strongly reduced at $B = 6$ T.

The increased allowedness of transition $I_B \rightarrow 0$ under application of a magnetic field should also be reflected in the emission decay time of substate I. In particular, the almost pure and long-lived triplet substate is expected to experience a distinct reduction of the emission decay time when mixing with shorter-lived substates occurs. Indeed, drastic effects are observed (Figure 8). At $T = 1.7$ K, the emission decay time of substate I decreases from $\tau_I = 133$ μs at $B = 0$ T to 20 μs at $B = 10$ T. The measurements were carried out with detection at the respective Zeeman shifted electronic origin (for $B = 0$ T at 16268 cm^{-1} and for $B = 10$ T at 16264.7 cm^{-1}). These data show clearly that a simple approach of taking into account only a mixing of the two lowest substates I and II is not successful, in contrast to the situation found for $Ir(ppy)_3$.[34] This is due to the observation that the decay time of I_B at $B = 10$ T is with $\tau_B = 20$ μs much shorter than the decay time of II at $B = 0$ T ($\tau_{II} = 58$ μs). Therefore, it has to be concluded that the Zeeman mixing occurs between all three substates. In particular, the singlet component of substate III is responsible for the drastic shortening of the emission decay time of the lowest substate by the applied high magnetic field.

The Zeeman effects as described above are typical for three substates of one parent T_1 term. Thus, the magnetic field behavior gives direct evidence that the three lines I, II, and

III cannot be related to different sites, but represent emissions from one specific site (site H).

4. Assignments and Conclusion

In the preceding sections, the lowest T_1 state of Ir(btp)$_2$(acac) and its splitting into substates I, II, and III has been investigated, in particular for one specific site (site H) in CH_2Cl_2. The three triplet substates have been identified from emission and excitation spectra. The electronic origins lie at 16268 cm^{-1} (I → 0), 16271 cm^{-1} (II → 0), and 16293 cm^{-1} (III → 0). Measurements under high magnetic field provide additional evidence for the triplet nature of the emitting substates. Moreover, the observed Zeeman interactions between the corresponding states prove directly that they result from one T_1 parent term of one specific site. If such investigations are not carried out, it is (due to the weakness of transition I → 0 and the small splitting between substates I and II) easily possible to misinterpret the occurring line structure. As consequence, a reliable characterization of the triplet cannot succeed. The total zero-field splitting (of site H) amounts to 25 cm^{-1}. This information carries an important message. In refs 3, 39, and 48−50 it was shown that the amount of zero-field splitting displays the extent of MLCT perturbation of the emitting state T_1. Significant splitting of a triplet state is only present if spin−orbit coupling induced by the heavy metal ion is effective and provides mixing of the triplet substates with higher lying triplets and singlets.[45,46] The mixing is not only responsible for the splitting of the lowest triplet into substates, but (beside a variation of many other photophysical properties[3]) also for a softening of the spin forbiddenness of transitions from triplet substates to the singlet ground state 0 and, in particular, for an increase of the radiative rate and a reduction of the emission decay times. An empirical ordering scheme recently developed by Yersin et al.[3,39,45,48−50] for organo-transition-metal triplet emitters provides a useful scale for an assessment of the MLCT parentage in the T_1 state according to its zero-field splitting. This ordering scheme, involving a large number of compounds, has already been utilized for the classification of the lowest triplet state of the well-known Ir(ppy)$_3$, which exhibits a large zero-field splitting of 83 cm^{-1} in THF.[34] Therfore, its emitting triplet is dominated by large MLCT parentage. Correspondingly, a high degree of MLCT character has also been calculated for Ir(ppy)$_3$ in the theoretical works of Hay[51] and Nozaki.[46] Other examples of emitters with strong MLCT components are $[Ru(bpy)_3]^{2+}$ (bpy = 2,2′-bipyridine) and $[Os(bpy)_3]^{2+}$ with zero-field splittings of the lowest triplet state of 60[48−50] and 210 cm^{-1},[49,50] respectively. In contrast, complexes such as Pd(2-thpy)$_2$ (thpy = (2-thienyl)pyridinate),[39,52,53] Pdq$_2$ (q = 8-hydroxyquinoline),[49] and Ptq$_2$,[49,54] as well as $[Rh(bpy)_3]^{3+}$ [55] and $[Pt(bpy)_2]^{2+}$,[48,50] are characterized by zero-field splitting values significantly below 1 cm^{-1}. They emit from only slightly perturbed ligand centered ^{3}LC states. The heteroleptic Ir(ppy)$_2$(CO)(Cl) with ZFS < 1 cm^{-1} [35] is a further representative of this class. The intermediate range is allocated by complexes with moderate ZFS values, such as Pt(2-thpy)$_2$[39,49,50] and Pt(ppy)$_2$[49,50] with 16 and 32 cm^{-1}, respectively. For Pt(2-thpy)$_2$, a corresponding assignment is also found by use of CASSCF/CASPT2 calculations.[53] Pt(Me$_4$salen) (salen = *N*,*N*′-bis(salicylidene)), which is a stable and highly efficient OLED emitter,[56] features a splitting of 17 cm^{-1} [57] and thus represents another example of the intermediate range. The emission of these complexes is assigned to result from ^{3}LC states with significant MLCT perturbations. The zero-field splitting of 25 cm^{-1} found for Ir(btp)$_2$(acac) also belongs to the intermediate range. Therefore, we classify the emitting state as a ligand centered (btp) $^3\pi\pi^*$ state with significant admixtures of MLCT character. The variation of the zero-field splitting values between 14.8 and 26.5 cm^{-1} found for the different sites of Ir(btp)$_2$(acac) in CH_2Cl_2 and for the different matrices (compare Table 1) and the distinct variation of the individual emission decay times (see ref 38) prove a significant influence also of the host environment on the emitting triplet state and the LC/MLCT admixture. For amorphous hosts, such as those usually used in OLEDs, we expect that the amount of ZFS will cover a similar range as found for the different sites of Ir(btp)$_2$(acac) in CH_2Cl_2, and thus, the photophysical properties of the emitter compound will vary correspondingly. Note that although higher radiative rates are expected to occur with increasing ΔE(ZFS), nonradiative processes are not considered here. Therefore, a direct correlation between MLCT perturbation and photoluminescence quantum yield is not possible. Yet the MLCT perturbation can be regarded as a necessary but not sufficient condition for complexes' usability in OLEDs.

In conclusion, it is remarked that the properties of the emitting triplet state of an organo-transition-metal compound strongly determine its suitability for application in OLEDs in terms of efficiency, emission decay time, color purity, etc. Therefore, a detailed characterization of such compounds will open new strategies for material development. In this respect, it should be mentioned that all good OLED triplet emitters hitherto studied exhibit zero-field splittings of the parent T_1 term larger than about 10 cm^{-1}.[45]

Acknowledgment. We thank the Bundesministerium für Bildung und Forschung (BMBF) for providing the funding of this investigation. The BaCaTeC is acknowledged for financial support of the exchange program of the University of Regensburg with the University of Southern California.

Note Added after ASAP Publication. This article was released ASAP on May 9, 2007, with a minor error in section 3.2. The correct version was posted on May 10, 2007.

IC0622860

(48) Yersin, H.; Humbs, W.; Strasser, J. *Coord. Chem. Rev.* **1997**, *159*, 325.
(49) Yersin, H.; Strasser, J. *J. Lumin.* **1997**, *72*−*74*, 462.
(50) Yersin, H.; Humbs, W.; Strasser, J. *Top. Curr. Chem.* **1997**, *191*, 153.
(51) Hay, P. J. *J. Phys. Chem. A* **2002**, *106*, 1634.
(52) Glasbeek, M.; Sitters, R.; van Veldhoven, E.; von Zelewsky, A.; Humbs, W.; Yersin, H. *Inorg. Chem.* **1998**, *37*, 5159.
(53) Pierloot, K.; Ceulemans, A.; Merchan, M.; Serrano-Andres, L. *J. Phys. Chem. A* **2000**, *104*, 4374.
(54) Donges, D.; Nagle, J. K.; Yersin, H. *Inorg. Chem.* **1997**, *36*, 3040.
(55) Glasbeek, M. *Top. Curr. Chem.* **2001**, *213*, 95.
(56) Che, C. M.; Chan, S. C.; Xiang, H. F.; Chan, M. C. W.; Liu, Y.; Wang, Y. *Chem. Commun.* **2004**, *13*, 1484.
(57) Lai, S. W.; Che, C. M.; Finkenzeller, W. J.; Yersin, H. In preparation.